

Model Studies on the Ozone-Mediated Synthesis of Cobalt Oxide Nanoparticles from Dicobalt Octacarbonyl in Ionic Liquids

Ralf Schuster,^[a] Tobias Wähler,^[a] Miroslav Kettner,^[a] Friederike Agel,^[b] Tanja Bauer,^{*[a]} Peter Wasserscheid,^[b, c] and Jörg Libuda^[a]

Low-temperature synthesis in ionic liquids (ILs) offers an efficient route for the preparation of metal oxide nanomaterials with tailor-made properties in a water-free environment. In this work, we investigated the role of 1-butyl-1-methylpyrrolidinium bis(trifluoromethylsulfonyl)imide [C₄C₁Pyr][NTf₂] in the synthesis of cobalt oxide nanoparticles from the molecular precursor Co₂(CO)₈ with ozone. We performed a model study in ultra-clean, ultrahigh vacuum (UHV) conditions by infrared reflection absorption spectroscopy (IRAS) using Au(111) as a substrate. Exposure of the pure precursor to ozone at low temperatures

results in the oxidation of the first layers, leading to the formation of a disordered Co_xO_y passivation layer. Similar protection to ozone is also achieved by deposition of an IL layer onto a precursor film prior to ozone exposure. With increasing temperature, the IL gets permeable for ozone and a cobalt oxide film forms at the IL/precursor interface. We show that the interaction with the IL mediates the oxidation and leads to a more densely packed Co_xO_y film compared to a direct oxidation of the precursor.

1. Introduction


Cobalt oxide holds the potential to replace noble metals in catalysis and energy technology. Potential fields of application are for example heterogeneous catalysis,^[1–3] energy storage,^[4–6] environmental catalysis,^[7,8] electrochemical water splitting^[9–13] and electrocatalysis.^[14] Two stable cobalt oxide structures are known: Co₃O₄ and CoO, exhibiting a spinel and a rock salt crystal structure, respectively. The most interesting properties of these oxides are the formation of hydroxyl species and the possibility to change the oxidation state of the cobalt ions by reduction or oxidation.^[15] The latter two processes release


oxygen from the surface or consume oxygen, respectively. It is important to note that the catalytic activity and properties are critically defined by the termination of the crystalline facets, which may expose Co²⁺, Co³⁺ or O²⁻ ions. Therefore, it is of particular interest to establish reliable synthesis routes with a high level of structural control to produce task-specific cobalt oxide nanomaterials. One promising route is the low-temperature synthesis in ionic liquids (ILs). ILs serve as stabilizers or structure-directing agents to control shape, size, and crystal structure during the synthesis of metal(oxide) nanoparticles (NPs). Moreover, the use of ILs as solvents during oxide synthesis omits the formation of hydroxides and in consequence high temperature calcination steps, which might induce structural changes in the obtained material.^[16–20] In addition, ILs enable to study such syntheses under controlled ultra-high vacuum (UHV) conditions, due to their negligible vapor pressure.^[21] By variation of anion/cation combinations as well as functionalization patterns, ILs offer a large variety of reaction media. To fully exploit the unique chemical flexibility of ILs for a knowledge-driven design of synthesis routes, a detailed understanding of the IL/reactant interactions at the molecular level is crucial. Recently, we reported on an ozone-mediated route towards Co₃O₄ NPs on bench scale in a water-free IL environment at low temperatures.^[22] In particular, exposure of the cobalt precursor Co₂(CO)₈ in [C₄C₁Pyr][OTf] to ozone leads to the formation of Co₃O₄ NPs with a narrow size distribution and an average size of 4 nm. The monocrystalline nature of the nanoparticulate product was proven by X-ray diffraction (XRD) and transmission electron microscopy (TEM). Additionally, we monitored the synthesis in situ by infrared reflection absorption spectroscopy (IRAS) in thin film configuration. It was shown that the reaction proceeds via a fast loss of the CO ligands followed by a slower formation of Co₃O₄ without observation of

[a] R. Schuster, T. Wähler, Dr. M. Kettner, Dr. T. Bauer,* Prof. J. Libuda
Interface Research and Catalysis, Erlangen Center for Interface Research
and Catalysis (ECRC)
Friedrich-Alexander-Universität Erlangen-Nürnberg
Egerlandstraße 3
91058 Erlangen (Germany)
Tel: +49 9131 85 67663
E-mail: tanja.tb.bauer@fau.de

[b] Dr. F. Agel, Prof. P. Wasserscheid
Institute of Chemical Reaction Engineering
Friedrich-Alexander-Universität Erlangen-Nürnberg
Egerlandstr. 3
91058 Erlangen (Germany)

[c] Prof. P. Wasserscheid
Forschungszentrum Jülich,
„Helmholtz-Institute Erlangen-Nürnberg for Renewable Energies“ (IEK 11)
Egerlandstr. 3
91058 Erlangen (Germany)

 An invited contribution to a Special Issue dedicated to Material Synthesis in Ionic Liquids

 © 2020 The Authors. Published by Wiley-VCH GmbH. This is an open access article under the terms of the Creative Commons Attribution Non-Commercial NoDerivs License, which permits use and distribution in any medium, provided the original work is properly cited, the use is non-commercial and no modifications or adaptations are made.

intermediates or byproducts. In the present work, we scrutinize the earliest stages of this process, i.e. the interaction between the IL, $\text{Co}_2(\text{CO})_8$, and ozone, to provide a molecular-level understanding of the influence of the IL on the nanoparticle formation. To this end, we prepared thin films of $[\text{C}_4\text{C}_1\text{Pyr}][\text{NTf}_2]$ and $\text{Co}_2(\text{CO})_8$ in different deposition orders on Au(111) in UHV environment and exposed them to thermal treatment and/or ozone. All steps are monitored by surface IRAS. Our experiments show that oxidizing and/or thermal treatment converts the cobalt carbonyls to Co_xO_y and/or Co nanoclusters. An IL coating protects the underlying precursor molecules against oxidation with ozone at low temperatures. In general, interaction of the precursor molecules with Au(111) is stronger compared to the interaction with the IL.

Experimental Section

Experimental Setup and Time-Resolved IRAS Experiments

All IRAS measurements were performed in a UHV setup with a base pressure of $1.5 \cdot 10^{-10}$ mbar. A detailed description can be found elsewhere.^[23] IR spectra were acquired using a Fourier-transform infrared (FTIR) spectrometer (Bruker Vertex 80v) with an external Liquid-Nitrogen-cooled-Mercury-Cadmium-Telluride (LN-MCT) detector. Both spectrometer and detector are connected to the UHV chamber via differentially pumped CsI windows. During the thin film preparation, spectra were continuously recorded with an acquisition time of 60 s per spectrum and a spectral resolution of 4 cm^{-1} . All spectra were referred to a background spectrum (4 cm^{-1} , 20 min) recorded on the clean Au(111) surface prior to the deposition.

Temperature-Programmed IRAS Experiments

For the TP-IRAS experiments, IR spectra were continuously recorded (60 s , 4 cm^{-1}) while a heating rate of 2 K/min was applied to the surface. The recorded data were analyzed using a procedure proposed by Xu et al.^[24] This procedure corrects for signal intensity losses due to the decreasing reflectivity of the surface with increasing temperature. The recorded background spectrum of the clean Au(111) surface was used as a reference for the corrected TP-IRAS spectra.

Preparation of the Au(111) Single Crystal

The Au(111) single crystal (MaTeck GmbH, purity 99.999%) was cleaned by Ar^+ sputtering (1.65 keV , 300 K , 60 min , $5 \cdot 10^{-5}$ mbar, Linde 6.0). Subsequently, annealing in UHV at 923 K for 5 min forms a well-ordered surface. This was proven by low energy electron diffraction (LEED).

Deposition of $\text{Co}_2(\text{CO})_8$

The volatile precursor was stored in a glass vial connected to a fine leak valve and a stainless-steel tube, separated from the UHV chamber via a gate valve and pumped by a separate bypass-system. Before each deposition, the tube was brought in close proximity to the Au(111) surface to ensure a localized deposition.

Physical Vapor Deposition of $[\text{C}_4\text{C}_1\text{Pyr}][\text{NTf}_2]$

The IL was evaporated from a glass crucible using a home-built thermal evaporator. This evaporator was separated from the UHV chamber by a gate valve and was pumped by a separate bypass-system. Before each deposition, the IL was pre-heated for 60 min at 443 K to get rid of possible contaminations. The thickness of the prepared IL films ranges between 1–2 monolayers (ML) (experiments at 225 K) and 4–6 ML (experiments at 110 K).

Ozone Dosage

Ozone was generated from O_2 (Linde, 5.0) using a commercially available ozone generator (COM-AD-01, Anseros GmbH) in combination with a home-built gas dosing system. A detailed description can be found elsewhere.^[16] In brief, the design ensures expansion of the gas into the UHV chamber with the sample in line-of-sight and a short residence time in the gas lines. The ozone content in the gas stream was adjusted for the individual exposures and measured with an ozone gas analyzer (GM-OEM, Anseros GmbH). The maximum ozone content in the feed ($80\text{--}90 \text{ g/m}^3$) was applied if not stated otherwise.

2. Results and Discussion

2.1. Deposition of $\text{Co}_2(\text{CO})_8$ and $[\text{C}_4\text{C}_1\text{Pyr}][\text{NTf}_2]$ Layered Films on Au(111) at 110 K

In the following, we investigate the growth of $\text{Co}_2(\text{CO})_8$ and $[\text{C}_4\text{C}_1\text{Pyr}][\text{NTf}_2]$ layered films on a clean Au(111) surface. To that aim, we applied different deposition orders of the IL and the precursor and monitored the growth of multilayers at 110 K by time-resolved IRAS. For a depiction of all recorded spectra during the preparation of the two layered films, please refer to Figure S1 of the Supporting Information.

First, we scrutinize the deposition of $\text{Co}_2(\text{CO})_8$ followed by $[\text{C}_4\text{C}_1\text{Pyr}][\text{NTf}_2]$ on Au(111). Selected spectra are shown in Figure 1a (left panel), while the complete data set is shown in the Supporting Information (Figure S1). At low coverage of the precursor, a peak emerges at 2056 cm^{-1} with a shoulder at 2044 cm^{-1} . With increasing coverage, a new sharp signal appears at 2093 cm^{-1} together with a broad, less intense shoulder at 2075 cm^{-1} . Additionally, we observe a band at 2113 cm^{-1} . A higher surface coverage leads to the formation of a broad feature at $\sim 1850 \text{ cm}^{-1}$. Eventually, this band transforms into a broad peak at 1847 cm^{-1} with a shoulder at 1812 cm^{-1} , while the other signals grow in intensity. Various studies on the IR vibrations of $\text{Co}_2(\text{CO})_8$ and its possible decomposition products have been performed in the last decades. Noack and Bor showed that the intact $\text{Co}_2(\text{CO})_8$ precursor has at least two isomers.^[25–27] Isomer 1 features two bridging CO ligands while Isomer 2 exclusively contains terminal CO ligands. The fraction of Isomer 2 in a hydrocarbon solution at room temperature was estimated to be around 40%. A depiction of the different isomers is included in Table 1. By studying matrix-isolated $\text{Co}_2(\text{CO})_8$, Sweany and Brown proved the existence of Isomer 3, which also only contains terminal CO ligands.^[28] Conversion of Isomer 3 into Isomer 2 is facile, while the conversion of Isomer 1 into Isomer 2 has a higher activation barrier, but is still

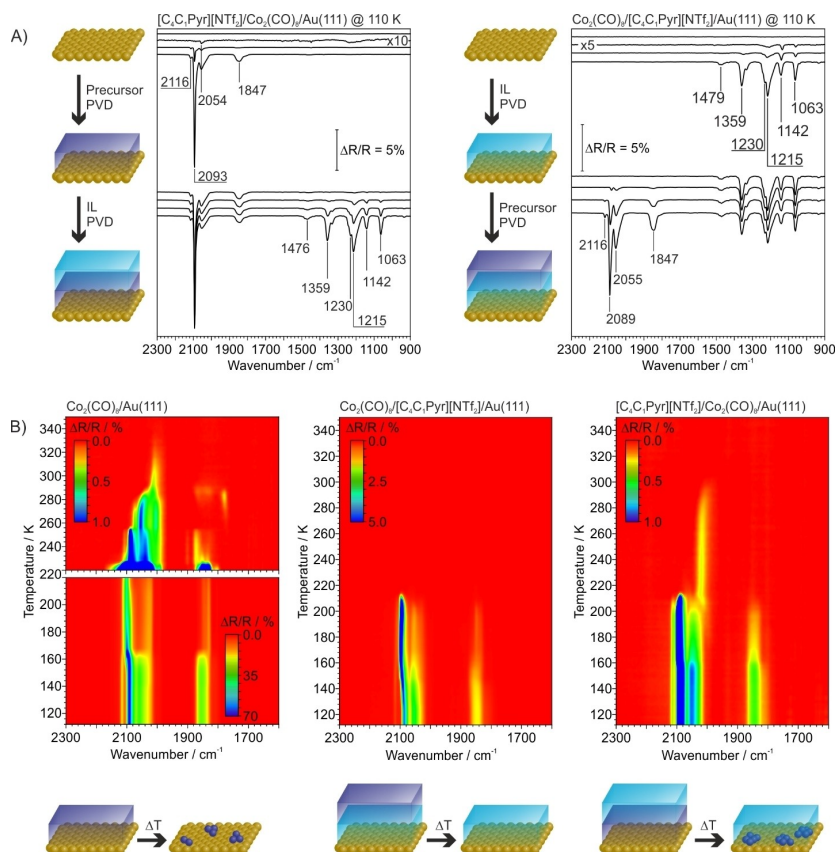
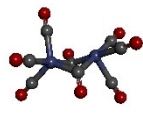
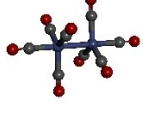

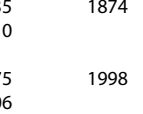

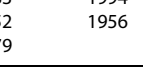
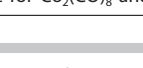


Figure 1. Film preparation at 110 K and thermal stability: A) Evaporation of $Co_2(CO)_8$ on Au(111) followed by PVD of $[C_4C_1Pyr][NTf_2]$ (left panel) and the reversed deposition order (right panel); B) from left to right: temperature-programmed IRAS recorded on $Co_2(CO)_8/Au(111)$, $Co_2(CO)_8/[C_4C_1Pyr][NTf_2]/Au(111)$ and $[C_4C_1Pyr][NTf_2]/Co_2(CO)_8/Au(111)$.

Table 1. Overview over the CO stretch vibrations of the different cobalt carbonyl complexes reported in literature. The band positions are given in cm^{-1} .								
	DFT ^[35] / Structure	Alkane ^{a-[25,29]}		Solution ^[32]		Ar Matrix ^[28]		ortho-dichlorbenze ^[34]
$Co_2(CO)_8$ Isomer 1		2112	2035	2475	2024	2117		
		2071	2021	2326	1992	2076	1868	2070
		2044	1867	2105	1860	2050	1857	2040
		2042	1857	2068	1825	2048		2022
$Co_2(CO)_8$ Isomer 2		2106				2074	2030	
		2069	2022			2052	2026	
		2031	1991					
$Co_2(CO)_8$ Isomer 3		2059 ^[26,27]				2059	2032	
		1991 ^[26,27]				2043	2002	
$Co_4(CO)_{12}$		2037	2104	2037	2110	1905		2057
		2035	2063	1898	2058	1873		2011
		2010	2054	1866	2030	1838		
$Co(CO)_4$					1996			
		2075	1998					2011
$HCo(CO)_4$		2006						
		2082	2000		2119	1996		
		2032			2070	1957		
$Co(CO)_3$ $Co(CO)_2$ $CoCO$					2053	1934		
		2083	1994		2030			
		2052	1956					

[a] Alkane is n-hexane for $Co_2(CO)_8$ and n-pentane for $Co_4(CO)_{12}$.

occurring at room temperature. It is important to note that $\text{Co}_2(\text{CO})_8$ is thermodynamically unstable in the absence of CO, however, the conversion to the stable decomposition product $\text{Co}_4(\text{CO})_{12}$ is kinetically hindered below room temperature.^[29,30] At room temperature, the thermal conversion into $\text{Co}_4(\text{CO})_{12}$ has a half-life period of approximately 9 hours in solution and, thus, some $\text{Co}_4(\text{CO})_{12}$ may be already present in the crucible prior to evaporation.^[31] Furthermore, homo- and heterolytic splitting of the Co–Co bond as well as release of CO ligands can occur on the gold surface, leading to possible $\text{Co}(\text{CO})_n$ ($n = 1-4$) radicals or anions, respectively.^[25,28,29,32-35] Additionally, the loss of all carbonyl ligands can lead to the formation of metallic cobalt.

In accordance with these findings we tentatively assign the bands at 2056 cm^{-1} and 2044 cm^{-1} to stretching vibrations of terminal CO ligands of Isomer 3. However, the presence of Isomer 1 or $\text{Co}_4(\text{CO})_{12}$ at low coverages cannot be ruled out solely based on the absence of vibrations of bridging CO ligands. Due to the metal surface selection rule (MSSR), vibrations with a dynamic dipole moment oriented parallel to the surface cannot be probed by IRAS.^[36-38] If all $\text{Co}_4(\text{CO})_{12}$ molecules adopt an adsorption geometry, in which the dipole moment of the stretching vibrations of bridging CO ligands is oriented parallel to the surface, one would only observe the stretching vibrations of the terminal CO ligands. Based on the absence of vibrations below 2000 cm^{-1} , we suggest that no mononuclear cobalt carbonyl fragments are formed. Signals at 2075 cm^{-1} , 2093 cm^{-1} and 2113 cm^{-1} , which emerge at increasing coverages, are assigned to terminal CO ligands of Isomer 2. The peak at 1850 cm^{-1} , emerging at higher surface coverages, is characteristic for a stretching vibration of a bridging CO ligand, which is only present in $\text{Co}_4(\text{CO})_{12}$ or Isomer 1. Overall, evaluation of the spectra indicates the presence of $\text{Co}_2(\text{CO})_8$ and possibly $\text{Co}_4(\text{CO})_{12}$ on the surface, which proves the deposition of these cobalt carbonyls on Au(111) at 110 K.

Subsequently, a multilayer of $[\text{C}_4\text{C}_1\text{Pyr}][\text{NTf}_2]$ was evaporated on top of the as-deposited precursor film. PVD of $[\text{NTf}_2]^-$ -based ILs has been thoroughly studied by our group, including coverage- and temperature-induced changes in the spectra.^[39-42] Briefly, the organic cations give rise to weak features above 1400 cm^{-1} , whereas the $[\text{NTf}_2]^-$ anions lead to strong, characteristic IR bands in the region from 1000 to 1400 cm^{-1} (for assignment see Table 2). In particular, evaluation of the intensity distribution of $\nu(\text{SO}_2)_{\text{as}}$, $\nu(\text{CF}_3)_{\text{as}} + \nu(\text{SO}_2)_{\text{sr}}$ and $\nu(\text{SNS})_{\text{as}}$ vibrations of $[\text{NTf}_2]^-$ allows to deduce the orientation and conformation of the anions on a surface.^[39-42]

Wavenumber [cm^{-1}]	Assignment ^[42]
1470–1480	$\delta(\text{CH}_2)$
1342–1360	$\nu(\text{SO}_2)_{\text{as}}$
1225–1230	$\nu(\text{SO}_2)_{\text{s}} + \nu(\text{CF}_3)_{\text{s}}$
1214–1215	$\nu(\text{SNS})_{\text{as}} + \nu(\text{CS}) + \nu(\text{CF}_3)_{\text{s}}$
1138–1145	$\nu(\text{CF}_3)_{\text{as}} + \nu(\text{SO}_2)_{\text{s}}$
1061–1067	$\nu(\text{SNS})_{\text{as}}$

In the present case, the band at 1145 cm^{-1} ($\nu(\text{CF}_3)_{\text{as}} + \nu(\text{SO}_2)_{\text{s}}$) is more pronounced as compared to the band at 1347 cm^{-1} ($\nu(\text{SO}_2)_{\text{as}}$) at low coverages. By considering the MSSR, we propose that the anions adopt a rather parallel orientation at the IL/precursor interface. Increasing the IL coverage leads to an intensity distribution characteristic for an unordered multilayer.^[42] During deposition of the IL layer, the overall intensity of the precursor signals decreases. This effect is attributed to the desorption of weakly bound precursor molecules upon IL adsorption, which indicates a weak precursor/metal interaction at this temperature.

In a corresponding experiment, multilayers of $[\text{C}_4\text{C}_1\text{Pyr}][\text{NTf}_2]$ and $\text{Co}_2(\text{CO})_8$ were deposited on clean Au(111), which results in a reversed deposition order (Figure 1a right panel). Again, the signal at 1350 cm^{-1} ($\nu(\text{SO}_2)_{\text{as}}$) is more intense than the features at 1139 cm^{-1} ($\nu(\text{CF}_3)_{\text{as}} + \nu(\text{SO}_2)_{\text{s}}$) and at 1061 cm^{-1} ($\nu(\text{SNS})_{\text{as}}$). This indicates a parallel adsorption geometry of the anions with the two SO_2 groups binding to the gold surface. At higher coverages, the intensity distribution of the signals is characteristic for a randomly orientated multilayer, as observed in the literature.^[42] Subsequently, a multilayer of $\text{Co}_2(\text{CO})_8$ was evaporated on top of the IL. Uptake of the precursor leads to a decrease of the intensity of all IL signals, indicating desorption of weakly bound IL molecules. At low precursor coverage, new signals evolve at 1850 cm^{-1} , 2051 cm^{-1} and 2078 cm^{-1} . Increase of the precursor coverage leads to an overall gain in signal intensity and the formation of a new peak at 2116 cm^{-1} . At higher coverages, the peak at 2078 cm^{-1} shifts to 2089 cm^{-1} , while the shift for the other peaks is negligible. The occurrence of peaks at 1850 cm^{-1} , 2051 cm^{-1} and 2078 cm^{-1} at the onset of the deposition suggests the presence of Isomer 1 or $\text{Co}_4(\text{CO})_{12}$ directly after the start of the deposition. This is in contrast to the deposition of $\text{Co}_2(\text{CO})_8$ onto pristine Au(111), where peaks originating from bridging CO ligands are observed at high precursor coverages only. There are two possible explanations for this effect. Either contact to the Au(111) surface facilitates the conversion of Isomer 1 and $\text{Co}_4(\text{CO})_{12}$ to cobalt carbonyls with exclusively terminal CO ligands (Isomer 2 and Isomer 3 or fragments), or the adsorption geometry of precursor molecules is different on Au(111) as compared to $[\text{C}_4\text{C}_1\text{Pyr}][\text{NTf}_2]/\text{Au}(111)$. In the latter scenario, the precursor molecules would adopt a rather random orientation on the IL. Even though the peak positions of the precursor bands match almost the ones observed for the $[\text{C}_4\text{C}_1\text{Pyr}][\text{NTf}_2]/\text{Co}_2(\text{CO})_8/\text{Au}(111)$ film, the relative contribution of the signals differs strongly. This indicates that the deposited precursor layers are composed of different molecular species on Au(111) and $[\text{C}_4\text{C}_1\text{Pyr}][\text{NTf}_2]$. We suggest that Au(111) promotes the conversion of bridged carbonyl complexes to isomers with exclusively terminal-bound ligands. The fact that no interconversion is observed in case of precursor molecules deposited on $[\text{C}_4\text{C}_1\text{Pyr}][\text{NTf}_2]$ indicates that the IL/precursor interaction is weaker compared to the metal/precursor interaction.

2.2. Thermal Stability of $\text{Co}_2(\text{CO})_8$ and $[\text{C}_4\text{C}_1\text{Pyr}][\text{NTf}_2]$ Layered Films on Au(111)

In this section, the thermal behavior of the prepared films is studied by temperature-programmed (TP-)IRAS. Please note that according to the results presented above, the layered films consist of mostly intact cobalt carbonyl (Isomers 1–3 and possibly $\text{Co}_4(\text{CO})_{12}$) and IL multilayers. For comparison, we additionally investigate the behavior of a pure precursor multilayer on Au(111). In every experiment, the sample temperature was increased from 110 K to 350 K with a heating rate of 2 K/min while continuously recording IR spectra. The corresponding data for the samples is shown in Figure 1b. Note that the IL film is stable in this temperature range. Schuschke et al. showed, that the IL multilayer remains on the surface up to 380 K while multilayer desorption occurs between 380 and 400 K.^[42] Therefore, only the precursor bands will be discussed in the following. At first, the results of the $\text{Co}_2(\text{CO})_8/\text{Au}(111)$ film are discussed. The color-coded intensity plot is shown in Figure 1b (left panel). It is divided into two parts with different intensity scales to be able to visualize also small changes in intensity, which occur at elevated temperatures. All peaks are stable up to approximately 160 K, where the most sudden variations are found. The $\nu(\text{CO})$ modes of bridging and terminal CO ligands at around 1840 cm^{-1} , 2060 cm^{-1} , and 2093 cm^{-1} decrease in intensity. Additionally, the peak at 2093 cm^{-1} shifts to 2099 cm^{-1} . The vibrational band at 2116 cm^{-1} partially overlaps with this shifting band. Between 210 K and 228 K, we observe a strong decrease in intensity of all vibrational bands. We attribute this effect to the desorption of the weakly bound multilayer of precursor molecules. Heating to 220 K leads to a steady decrease of the feature at 2099 cm^{-1} while the other bands remain unaffected. Due to the generally large width of the peaks it is not possible to draw conclusions on the behavior of the different isomers ($\text{Co}_2(\text{CO})_8$ and $\text{Co}_4(\text{CO})_{12}$). However, our observation shows that thermally-induced changes in the structure of the layer occur already below multilayer desorption. After desorption of the physisorbed precursor multilayer, only the more strongly bound species in the monolayer region remain on the surface. Therefore, only weak bands at 2087 cm^{-1} , 2037 cm^{-1} , 2005 cm^{-1} , 1871 cm^{-1} , 1853 cm^{-1} , and 1835 cm^{-1} are observed. At 254 K, the peak at 2087 cm^{-1} and the remaining signals of bridged CO ligands at $1800\text{--}1900\text{ cm}^{-1}$ disappear. The band at 2037 cm^{-1} shifts to 2055 cm^{-1} . Upon further heating, the signal at 2055 cm^{-1} shifts to lower wavenumbers again and new signals emerge in the region characteristic for bridge-bonded CO at 1772 cm^{-1} and 1850 cm^{-1} . Above 290 K, only a single band at 2014 cm^{-1} is present in the spectra. This feature decreases in intensity without shifting and eventually disappears at 334 K.

The intensity variations of bands related to the bridging and terminal CO ligands indicate a dynamic conversion of bridged into non-bridged cobalt carbonyls. Above 254 K, only Isomer 2 and Isomer 3 of $\text{Co}_2(\text{CO})_8$ remain on the surface. However, the reappearance of vibrations at 1850 cm^{-1} at 280 K can be explained by the transformation of both species back to Isomer 1 or their thermal decomposition to $\text{Co}_4(\text{CO})_{12}$. A signal at such low wavenumbers as 1772 cm^{-1} was not observed before for

these compounds. It is noteworthy that the bands assigned to the intact precursor molecules in the monolayer are stable up to approximately 290 K on Au(111). The feature at 2014 cm^{-1} , which is formed above 290 K, is characteristic for CO adsorbed on metallic cobalt.^[43] However, no coverage-dependent shift is observed. Thus, we suggest that very small cobalt nanoclusters are formed on Au(111) via thermal decomposition of the precursor molecules.

Next, we analyze the thermal behavior of the $\text{Co}_2(\text{CO})_8/[\text{C}_4\text{C}_1\text{Pyr}][\text{NTf}_2]/\text{Au}(111)$ sample, i.e. deposition of the precursor on top of a pre-adsorbed IL layer. The corresponding color-coded intensity plot is shown in Figure 1b (central panel). All vibrational bands are stable up to 126 K. The features at 1850 cm^{-1} and 2054 cm^{-1} decrease in intensity upon heating to 170 K, while the signals at 2087 cm^{-1} and 2116 cm^{-1} gain in intensity. As for the $\text{Co}_2(\text{CO})_8/\text{Au}(111)$ film, the peak at 2087 cm^{-1} shifts to higher wavenumbers, leading to an overlap of the signals at 2097 cm^{-1} and 2116 cm^{-1} . Further heating leads to a strong overall decrease in peak intensity, which is attributed to the desorption of the precursor multilayer. Above 214 K, no further CO stretching vibrations are observed. Again, we attribute the simultaneous decrease of signals assigned to bridging CO ligands ($<1900\text{ cm}^{-1}$) and increase of bands characteristic for terminal CO ligands ($>2000\text{ cm}^{-1}$) to the conversion of bridged into non-bridged cobalt complexes. The fact that the desorption of the precursor occurs molecularly, i.e. without the formation of metallic cobalt and at significantly lower temperatures compared to $\text{Co}_2(\text{CO})_8/\text{Au}(111)$, strengthens our hypothesis that the IL/precursor interaction is weak compared to the metal/precursor interaction. However, the changes in the multilayer are highly pronounced in both samples.

Finally, the thermal behavior of $[\text{C}_4\text{C}_1\text{Pyr}][\text{NTf}_2]/\text{Co}_2(\text{CO})_8/\text{Au}(111)$ is discussed, i.e. deposition of the IL on top of a pre-adsorbed precursor layer. The corresponding data is shown in Figure 1b (right panel). All signals remain unchanged up to 152 K. Above this temperature, the bands at 1845 cm^{-1} and 2056 cm^{-1} continuously decrease in intensity. In contrast to the corresponding experiment with the reversed ordering, the bands at 2092 cm^{-1} and 2116 cm^{-1} show negligible intensity changes and peak shifts upon heating. At 214 K, the precursor bands strongly decrease in intensity and only a newly formed peak at 2015 cm^{-1} is visible in the spectra. This peak gains in intensity and shifts to higher wavenumbers, reaching 2022 cm^{-1} at 218 K. Further heating leads to a slow decrease of the peak intensity and a shift of the peak position to 1999 cm^{-1} at 298 K. Above 300 K, no bands are visible in the CO region of the IR spectra. The band at 2015 cm^{-1} is again assigned to CO adsorbed on metallic cobalt. We propose the formation of cobalt nanoclusters from the cobalt precursor after desorption of the weakly bound multilayer, due to the comparatively strong metal/precursor interaction on Au(111).^[43] No interconversion of bridged to non-bridged isomers is observed. We suggest that the IL cover layer further enhances the metal/precursor interaction as compared to the IL-free film. This leads to a larger amount of cobalt adatoms on the gold surface, which eventually agglomerate to small cobalt nanoclusters. This

hypothesis is strengthened by the observation that intact cobalt precursor species are present on Au(111) at temperatures up to 300 K, whereas in the case of the IL-covered sample exclusively CO bound to metallic cobalt is observed above 220 K. Note that these nanoclusters are bigger in comparison to the ones formed on the $\text{Co}_2(\text{CO})_8/\text{Au}(111)$ film without IL.

2.3. Exposure of $\text{Co}_2(\text{CO})_8$ and $[\text{C}_4\text{C}_1\text{Pyr}][\text{NTf}_2]$ Layered Films to Oxygen and Ozone at 110 K

In the following, we study the stability of the layered films against oxygen and ozone. Therefore, two freshly prepared films (for preparation see Section 2.1) were exposed to a constant background pressure ($2.5 \cdot 10^{-6}$ mbar) of oxygen and, subsequently, to ozone in oxygen at 110 K. In Figure 2a, the last spectrum recorded under each gas atmosphere is shown for $\text{Co}_2(\text{CO})_8/[\text{C}_4\text{C}_1\text{Pyr}][\text{NTf}_2]/\text{Au}(111)$ (left panel) and $[\text{C}_4\text{C}_1\text{Pyr}][\text{NTf}_2]/\text{Co}_2(\text{CO})_8/\text{Au}(111)$ (right panel). Additionally, the integrated peak areas of selected bands in the characteristic region for bridged

(< 1900 cm^{-1}) and terminal CO ligands (> 2000 cm^{-1}) are shown as a function of time and gas composition. Additionally, all measured spectra are depicted in Figure S2 of the Supporting Information.

First, the stability against oxidation of the precursor-terminated layered film is scrutinized. Oxygen backpressure induces only small changes of the precursor bands. Exposure to ozone, however, leads to a strong decrease of the peak intensities. This decrease levels off over time and precursor bands are still observable after 19 min exposure to ozone. We attribute the small changes in oxygen atmosphere to desorption of weakly bound precursor molecules and the intensity losses in the presence of ozone to oxidation of precursor molecules to cobalt oxide. Apparently, ozone as a strong oxidizing agent is necessary to oxidize the precursor molecules at 110 K. This observation is in accordance with experiments reported in the literature, where it was shown that the parent carbonyl compounds $\text{Co}_2(\text{CO})_8$ and $\text{Co}_4(\text{CO})_{12}$ are stable against oxygen, while their decomposition products are very sensitive towards oxygen.^[29] We propose that the first few layers of the

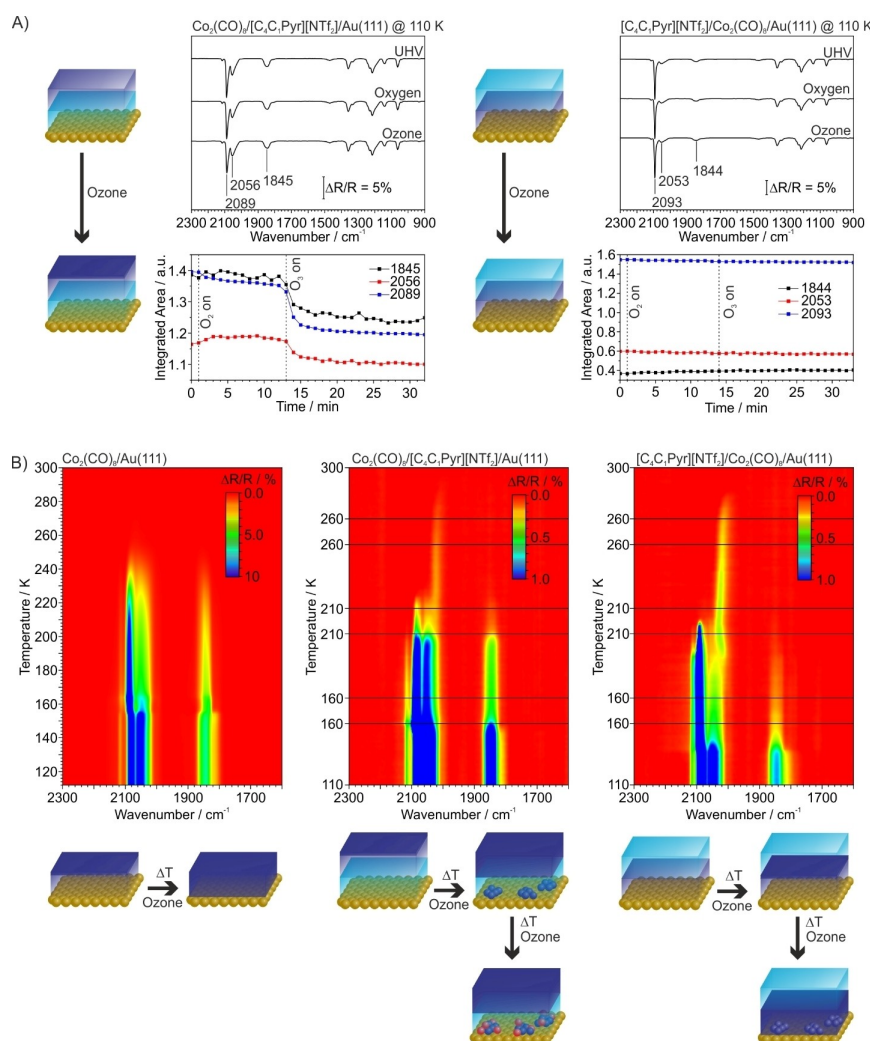


Figure 2. Stability against oxidation: A) Selected IR spectra after the exposure to oxygen and ozone of the two different films. Additionally, the integrated peak areas of selected CO vibration are shown as a function of time and gas composition; B) from left to right: temperature-programmed IRAS recorded on $\text{Co}_2(\text{CO})_8/\text{Au}(111)$, $\text{Co}_2(\text{CO})_8/[\text{C}_4\text{C}_1\text{Pyr}][\text{NTf}_2]/\text{Au}(111)$ and $[\text{C}_4\text{C}_1\text{Pyr}][\text{NTf}_2]/\text{Co}_2(\text{CO})_8/\text{Au}(111)$ films under a constant background pressure of ozone.

precursor are oxidized to a disordered Co_xO_y film. Ozone cannot further penetrate through this passivation layer and, thus, the underlying precursor molecules are protected against oxidation. No changes of the bands in the IL region are observed during this experiment.

Exposure of the IL-terminated film to oxygen leads only to a small desorption of IL while there is no influence of oxygen on the precursor bands. Even after 19 min of exposure to ozone in oxygen, we do not observe any changes in the precursor bands. This shows that ozone cannot penetrate the frozen IL layer, which protects the underlying precursor molecules against oxidation.

2.4. Thermal Stability of $\text{Co}_2(\text{CO})_8$ and $[\text{C}_4\text{C}_1\text{Pyr}][\text{NTf}_2]$ Layered Films Under Ozone

In the next step, we test the stability of the samples against oxidation by ozone at elevated temperatures in a TP-IRAS experiment. For comparison, we performed a similar experiment for a $\text{Co}_2(\text{CO})_8/\text{Au}(111)$ film. Each sample is exposed to ozone in oxygen at a background pressure of $\sim 4.0 \cdot 10^{-6}$ mbar while the surface temperature is increased by 2 K/min. In Figure 2b, the results for the different films are shown. While a constant temperature ramp was applied for the $\text{Co}_2(\text{CO})_8/\text{Au}(111)$ film (Figure 2b, left panel), the procedure is slightly modified in case of the layered samples (Figure 2b, central and right panel). The heating ramp was interrupted at 160 K, 210 K, and 260 K, where the respective temperature was kept constant for 600 s.

The IL bands are hardly affected by oxygen and/or ozone dosing at elevated temperatures, thus only bands related to the cobalt precursor will be discussed. At first, we focus on the $\text{Co}_2(\text{CO})_8/\text{Au}(111)$ film. No changes are observed upon heating to 150 K. Above 150 K, the broad feature in the bridging-CO region and the feature at 2054 cm^{-1} decrease in intensity and the peak shape becomes smaller and more defined. Simultaneously, the signal at 2083 cm^{-1} shifts to higher wavenumbers and increases in intensity by 60% at 160 K. Furthermore, the intensity of the signal at 2116 cm^{-1} increases in this temperature range. Further heating results in intensity losses of all features and above 268 K no molecular CO vibrations are observed. With respect to the TP-IRAS experiment in vacuo, spectral changes start to occur in a similar temperature range. The most striking difference is the intermediate gain in intensity of the features at 2083 cm^{-1} and 2116 cm^{-1} in the presence of ozone. We attribute this to a conversion of bridged complexes (Isomer 1 and $\text{Co}_4(\text{CO})_{12}$) into non-bridged precursor molecules (Isomer 2 and 3). A dynamic interconversion between $\text{Co}_2(\text{CO})_8$ isomers and $\text{Co}_4(\text{CO})_{12}$ was also observed by heating the sample in UHV, but only at significantly higher temperatures in the monolayer regime. Thus, our results suggest that interconversion in the multilayer is ozone-induced and that the conversion into non-bridged isomers is the first step towards the oxidation of the precursor to Co_xO_y . For the corresponding experiment under UHV a multilayer desorption temperature of around 225 K was observed, whereas the multilayer is present above this temper-

ature under ozone. This is explained by a stabilization of the multilayer by the covering oxide layer. Furthermore, vibrations of intact precursor molecules were observed even above 300 K in UHV, whereas in the presence of ozone no CO bands are observed above 268 K. In consequence, we propose that the initially formed passivation layer gets permeable for ozone at elevated temperatures, leading to a successive oxidation of the underlying precursor multilayer.

Next, the thermal behavior of the $\text{Co}_2(\text{CO})_8/[\text{C}_4\text{C}_1\text{Pyr}][\text{NTf}_2]/\text{Au}(111)$ film under ozone backpressure (Figure 2b, central panel) is discussed. All peaks are stable up to 150 K. Further heating leads to a loss of intensity of the broad feature at $1800\text{--}1880 \text{ cm}^{-1}$ together with the features at 2116 cm^{-1} and 2054 cm^{-1} . Simultaneously, the peak at 2088 cm^{-1} shifts to higher wavenumbers and gains in intensity at 152–160 K. Further heating leads to a constant loss of intensity. During the intermediate period of constant temperature at 210 K, an additional peak emerges at 2026 cm^{-1} . Above 220 K, this is the only signal remaining. A peak shift to 2007 cm^{-1} is observed with further increasing temperature and a decrease in intensity until the feature is completely lost at 284 K. The intermediate increase of the signal at 2088 cm^{-1} is again attributed to an ozone-induced transformation of bridged to non-bridged cobalt complexes. The emerging peak at 2026 cm^{-1} is assigned to CO adsorbates on cobalt nanoclusters. As discussed above, the formation of such cobalt aggregates is also observed during the TP-IRAS experiment of $[\text{C}_4\text{C}_1\text{Pyr}][\text{NTf}_2]/\text{Co}_2(\text{CO})_8/\text{Au}(111)$ under UHV. However, it did not occur in case of the precursor-terminated film under UHV, where heating led to molecular desorption of the weakly bound precursor molecules. Thus, the formation of cobalt nanoclusters on Au(111) must be related to ozone-induced changes of the layered film. In accordance with our previous findings, we propose the following: the reaction of the precursor with ozone leads to a continuous growth of a cobalt oxide passivation layer, which stabilizes the underlying precursor layers. At elevated temperature, metallic cobalt is formed upon thermal decomposition of the precursor and deposited on Au(111), due to increased mobility in the underlying IL layer. At this moment, it is not clear whether the abstraction of CO ligands occurs before or after contact of the cobalt species (molecular precursor or metallic cobalt, respectively) with the Au(111) surface. We will come back to this question below (see Section 2.5).

Finally, we discuss the thermal behavior of $[\text{C}_4\text{C}_1\text{Pyr}][\text{NTf}_2]/\text{Co}_2(\text{CO})_8/\text{Au}(111)$ under ozone. All peaks are stable up to 138 K. Increasing the temperature to 150 K leads to a decrease in intensity of the features at 1843 cm^{-1} and 2052 cm^{-1} while both peaks at 2115 cm^{-1} and 2093 cm^{-1} gain intensity. Between 152 K and 190 K only small intensity losses for the features at 2093 cm^{-1} and 2115 cm^{-1} are observed while the features in the bridged-CO region and at 2052 cm^{-1} lose in intensity. At 192 K, a new peak emerges at 2018 cm^{-1} and shifts to 2026 cm^{-1} with increasing temperature. Above 210 K, it is the only remaining band in the spectra. Upon further heating, the peak at 2026 cm^{-1} shifts to lower wavenumbers until it reaches 2003 cm^{-1} at 278 K and vanishes.

Two observations are of particular interest with respect to the temperature-dependent behavior of the sample in UHV and the results obtained from the layer film with the reverse order ($\text{Co}_2(\text{CO})_8/[\text{C}_4\text{C}_1\text{Pyr}][\text{NTf}_2]/\text{Au}(111)$) under ozone. First, the structural changes start at lower temperatures in the present experiment (138 K compared to 150 K). Secondly, no intensity loss of the bands at 2093 cm^{-1} and 2115 cm^{-1} between 150 and 190 K is observed. We propose that at 138 K the IL layer gets permeable for ozone. This induces interconversion of bridged to non-bridged isomers and oxidation of the underlying precursor molecules, which results in a Co_xO_y passivation layer at the IL/precursor interface. As further oxidation of the underlying precursor molecules only occurs above 190 K, we presume that the oxide film at the IL/precursor interface is more densely packed as compared to the passivation layer on a precursor-terminated film. The feature at 2026 cm^{-1} , which occurs above 192 K, is attributed to CO adsorbates on cobalt nanoclusters that are formed at the metal/precursor interface. Thus, heating under oxidizing conditions leads to the formation of cobalt oxide and metallic cobalt independent from the deposition order of the layered films at 110 K.

2.5. Deposition of $\text{Co}_2(\text{CO})_8$ and $[\text{C}_4\text{C}_1\text{Pyr}][\text{NTf}_2]$ on Au(111) at 225 K

Next, we performed the isothermal uptake experiment of $\text{Co}_2(\text{CO})_8$ and $[\text{C}_4\text{C}_1\text{Pyr}][\text{NTf}_2]$ at 225 K. This temperature was identified as the most interesting one in the TP-IRAS experiments starting at 110 K. It is close to the desorption temperature of the precursor multilayer, where previously also the formation of metallic cobalt was observed. Waterfall plots of all measured spectra during the preparation of the two layered films are shown in the Figure S3 of the Supporting Information.

First, we discuss the results obtained from the IL-covered precursor film. In Figure 3a (left panel), selected IR spectra of the evaporation of $\text{Co}_2(\text{CO})_8$ on clean Au(111) are shown followed by deposition of an IL layer. At the early stages of the precursor deposition, a peak emerges at 2036 cm^{-1} and shifts to 2073 cm^{-1} over time. As soon as the peak intensity saturates, two new features appear, i.e. a shoulder at 2087 cm^{-1} and another one at 2106 cm^{-1} . Both bands grow in intensity and an additional broad feature at 1871 cm^{-1} emerges. While the other peaks grow in intensity with increasing coverages, the intensity of the band at 2073 cm^{-1} stays constant, but a small shoulder occurs at 2031 cm^{-1} .

We assign the peak at 2036 cm^{-1} to stretching vibrations of CO adsorbates on cobalt nanoclusters. This is in good agreement with the previous temperature-dependent experiments, where we observed the formation of metallic cobalt at the metal/precursor interface above 200 K. The gradual shift of the band to higher wavenumbers results from an increasing CO surface coverage on these nanoclusters. The vibrational bands at 2087 cm^{-1} and 2106 cm^{-1} are assigned to terminal CO ligands of intact cobalt precursor molecules. As we do not observe signals of bridge-bonded CO at these low coverages, we attribute these bands to Isomer 2 or 3. This is in accordance

with the observations at 110 K, where only non-bridged complexes are present on Au(111) at low precursor coverage. This strengthens our assumption, that Au(111) facilitates the transformation of bridged to non-bridged precursor molecules. An additional feature at 1871 cm^{-1} , which is assigned to bridging CO ligands of Isomer 1 or $\text{Co}_4(\text{CO})_{12}$, is only visible at high coverages. We conclude that deposition of $\text{Co}_2(\text{CO})_8$ at 225 K leads to the formation of cobalt nanoclusters embedded in a multilayer of $\text{Co}_2(\text{CO})_8$ and $\text{Co}_4(\text{CO})_{12}$ on Au(111). Subsequently, the IL was deposited onto the precursor. At first, changes in the spectra occurring in the IL region ($900\text{--}1500\text{ cm}^{-1}$) are discussed. During the deposition of the IL, peaks emerge simultaneously at 1067 cm^{-1} , 1139 cm^{-1} , 1214 cm^{-1} , 1225 cm^{-1} , 1356 cm^{-1} , and 1480 cm^{-1} and grow linearly in intensity with increasing coverage. Since all bands start to grow simultaneously and show a linear growth behavior, the orientation of the molecules is independent on the IL coverage. However, the peak ratios differ from the ones obtained during deposition at 110 K (Figure 1a), where an unordered IL layer is formed on top of the precursor molecules. In the present experiment, bands with a contribution of the SO_2 stretch vibration (1139 cm^{-1} , 1225 cm^{-1} , and 1356 cm^{-1}) are less intense as compared to the bulk spectrum. We propose, therefore, that in the present experiment $[\text{NTf}_2]^-$ anions in the multilayer are preferentially oriented with the two oxygen atoms of each SO_2 group pointing towards the IL/precursor interface. The adsorption of the IL also induces changes of the carbonyl peaks. Except for the band at 2073 cm^{-1} , all bands lose 50 to 70% of their initial intensity. This is rationalized by the fact that the temperature of 225 K is close to the desorption temperatures of the precursor multilayer. Upon deposition of the IL, a large part of the precursor multilayer desorbs from the surface. The deposition of $[\text{C}_4\text{C}_1\text{Pyr}][\text{NTf}_2]$ has no influence on the CO adsorbates on cobalt nanoclusters.

Next, we discuss the results for the reversed deposition order. The obtained IR spectra are shown in Figure 3a (right panel). At low coverage of the IL on Au(111), the $\nu(\text{SNS})_{\text{as}}$ mode at 1061 cm^{-1} and the coupled $\nu(\text{CF}_3)_{\text{as}} + \nu(\text{SO}_2)_s$ mode at 1138 cm^{-1} are more intense as compared to the intensity distribution in a spectrum obtained from an unordered multilayer, while the $\nu(\text{SO}_2)_{\text{as}}$ mode at 1342 cm^{-1} is less pronounced. This suggests a preferred orientation of the molecules with both oxygen atoms of each SO_2 group binding to the surface. Upon further increase of the coverage beyond the monolayer regime, the spectra become more characteristic for a random oriented multilayer.^[42] This is in accordance to the observations of the experiments at 110 K, where the IL anions also adopt a random orientation distribution in the multilayer. However, the relative intensity ratios do not fit perfectly to the one for a random multilayer, which is due to the low total amount of IL deposited in this experiment. Subsequently, a precursor layer was deposited on top of the IL film. After long deposition of $\text{Co}_2(\text{CO})_8$ (61 min), a peak emerges at 2016 cm^{-1} . Upon further deposition, this peak shifts to 2035 cm^{-1} and gains in intensity. The feature was previously assigned to CO adsorbates on cobalt nanoclusters on Au(111). Either the precursor decomposes to metallic cobalt upon impingement on the IL-covered surface, or

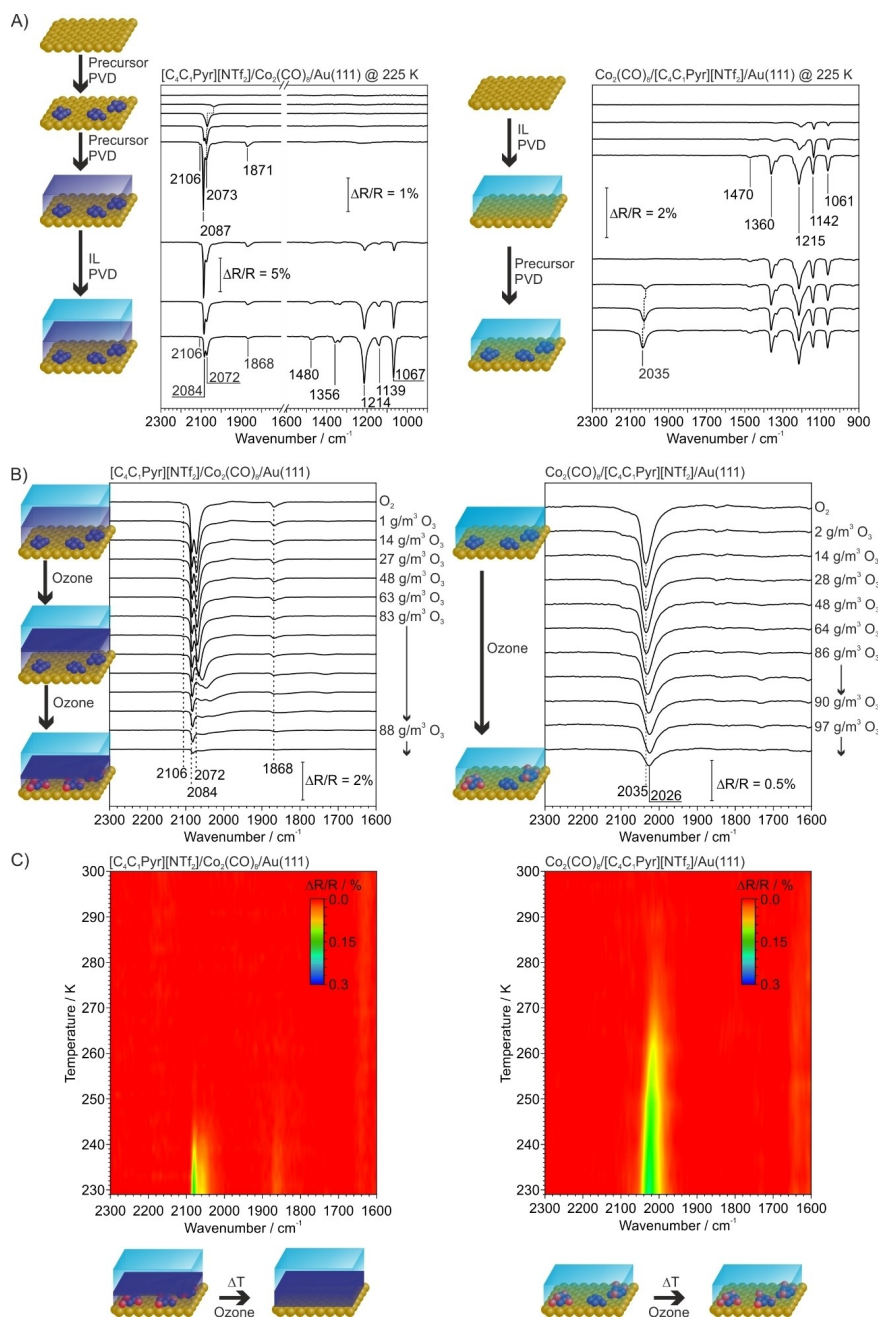


Figure 3. Experiments at 225 K: A) preparation of the two different layered films $[C_4C_1Pyr][NTf_2]/Co_2(CO)_8/Au(111)$ (left panel) and $Co_2(CO)_8/[C_4C_1Pyr][NTf_2]/Au(111)$ (right panel); B) exposure of the as prepared films to oxygen and increasing concentrations of ozone; C) temperature-programmed IRAS recorded on $[C_4C_1Pyr][NTf_2]/Co_2(CO)_8/Au(111)$ (left panel) and $Co_2(CO)_8/[C_4C_1Pyr][NTf_2]/Au(111)$ (right panel) under a constant background pressure of ozone.

it first diffuses through the IL layer towards the Au(111) surface, where it decomposes. There are no vibrations of molecular precursor complexes at 225 K, which is in line with the results from the TP-IRAS experiments under UHV (Figure 1b) and ozone (Figure 2b). Therefore, we propose that metallic cobalt and CO are formed on the IL film by decomposition of impinging precursor molecules. Both diffuse through the IL layer, forming CO covered cobalt nanoclusters on the gold surface. However, due to the diffusion and agglomeration process, the formation of the cobalt nanoclusters is slower as compared to direct deposition of the precursor onto Au(111). Interestingly, the

decomposition of precursor molecules and the formation of cobalt nanoclusters affect the orientation of the IL molecules. All bands grow in intensity except the one at 1142 cm^{-1} , which decreases. In the last spectrum, the shape and intensity distribution of the IL bands points towards the presence of randomly oriented anions.^[42] This indicates a reorientation of the molecules in the monolayer, induced by the formation of the cobalt nanoclusters on Au(111).

2.6. Exposure to Oxygen and Ozone

Subsequently, the two films were exposed to oxygen and ozone in oxygen at a constant background pressure of $2.3 \cdot 10^{-5}$ mbar. The respective spectra are depicted in Figure 3b. Additional plots are shown in the Supporting Information Figures S4 and S5. At first, we discuss the results for the $[\text{C}_4\text{C}_1\text{Pyr}][\text{NTf}_2]/\text{Co}_2(\text{CO})_8/\text{Au}(111)$. After recording a spectrum in UHV, the film was exposed to oxygen and increasing concentrations of ozone in oxygen. The bands assigned to CO ligands of the precursor molecules at 1871 cm^{-1} , 2087 cm^{-1} , and 2106 cm^{-1} decrease in intensity during the experiment. The most significant changes occur at an ozone concentration of 83 g/m^3 in the feed gas. As bands are still visible at 1862 cm^{-1} , 2060 cm^{-1} and 2080 cm^{-1} , not all precursor molecules are decomposed/oxidized. The signal at 2073 cm^{-1} , assigned to CO on cobalt nanoclusters, shows only minor changes under oxygen and ozone concentrations in the feed gas below 80 g/m^3 . At higher ozone concentrations, the peak shifts to 2016 cm^{-1} and decreases in intensity before it vanishes. At this temperature, the IL film is permeable for oxygen and ozone. In consequence, the top layer of the underlying precursor molecules is oxidized to Co_xO_y and a passivation layer is formed at the IL/precursor interface, indicated by the decrease of all precursor signals. Additionally, the disappearance of the peak at 2016 cm^{-1} indicates the loss of CO adsorbates from the nanoclusters. There are two possible explanations for this process. It can result from oxidation of CO to CO_2 by ozone (induced by ozone co-adsorption on Co) or the oxidation of the Co nanoclusters to Co_xO_y . We believe that the co-adsorption of ozone and the subsequent oxidation of the cobalt nanoclusters to Co_xO_y is more likely than the low temperature oxidation of carbon monoxide. The bands of the IL also show changes in intensity (see Figure S5 left panel in Supporting Information). In particular, the signals at 1139 cm^{-1} , 1225 cm^{-1} , and 1356 cm^{-1} increase in intensity while the other bands decrease. We interpret these changes as a reorientation of the IL molecules to a more random orientation, due to the changes of the underlying precursor layer.^[42]

Next, we analyze the results obtained for the layered film with the reversed deposition order $\text{Co}_2(\text{CO})_8/[\text{C}_4\text{C}_1\text{Pyr}][\text{NTf}_2]/\text{Au}(111)$. The peak at 2035 cm^{-1} shows only minor changes under oxygen and ozone concentrations below 28 g/m^3 in the feed gas. Above this concentration, the peak shifts to 2027 cm^{-1} and undergoes a loss in intensity, independent on a further increase of the ozone concentration. Compatible to the last experiment with the IL-terminated film, ozone exposure leads to the oxidation of the CO adsorbates or Co nanoclusters. In contrast to the exposure of the $[\text{C}_4\text{C}_1\text{Pyr}][\text{NTf}_2]/\text{Co}_2(\text{CO})_8/\text{Au}(111)$ sample to ozone, this feature does not completely disappear. This can be rationalized by the higher number of IL molecules per nanocluster in the present experiment. Either the larger amount of IL molecules inhibits co-adsorption of O_3 and therefore the oxidation of the nanoclusters or it stabilizes the CO adsorbates against oxidation. Only minor changes of the IL bands are observed due to desorption.

2.7. Subsequent Heating Under Ozone

Following the experiments presented in the last section, we continued to study the behavior of the resulting systems in a temperature-programmed experiment under ozone. To this aim, the background pressure of ozone was kept constant and the temperature was increased to 300 K with a heating rate of 2 K/min. The results are shown in Figure 3c. First, the color-coded intensity plot obtained for the film $[\text{C}_4\text{C}_1\text{Pyr}][\text{NTf}_2]/\text{Co}_2(\text{CO})_8/\text{Au}(111)$ will be discussed, see Figure 3c (left panel). In accordance with our findings from Section 2.6, we assume that the majority of the precursor is oxidized to Co_xO_y at the onset of the present experiment. With increasing temperature, the remaining peaks at 1862 cm^{-1} , 2060 cm^{-1} , and 2080 cm^{-1} lose intensity and disappear. Above 247 K, no CO vibrations are observable anymore. We propose that the remaining precursor species on the surface are oxidized to Co_xO_y at elevated temperature. As for the other TP-IRAS experiments, no ozone-induced changes of the IL bands are observed. We ascribe the small decrease of the IL bands to desorption of IL.

Finally, we analyze the thermal evolution of the remaining CO vibrations of the $\text{Co}_2(\text{CO})_8/[\text{C}_4\text{C}_1\text{Pyr}][\text{NTf}_2]/\text{Au}(111)$ film. The corresponding color-coded intensity plot is shown in Figure 3c (right panel). According to our findings from Section 2.6, we assume that a mixture of Co_xO_y and Co nanoclusters is present on Au(111) at the beginning of the experiment. The CO stretching vibration at 2027 cm^{-1} shifts by 17 cm^{-1} to lower wavenumbers and decreases in intensity with increasing temperature. These observations indicate the ongoing loss of CO bound to cobalt nanoclusters and show that the proposed protective function of the IL molecules on the cobalt nanoclusters is lost at elevated temperatures.

3. Conclusions

In this work, we studied the preparation, the thermal stability and the stability against oxidation of layered films of $\text{Co}_2(\text{CO})_8$ and $[\text{C}_4\text{C}_1\text{Pyr}][\text{NTf}_2]$ on Au(111) by time-resolved and temperature-programmed IRAS under UHV conditions. A graphical illustration of the observations for the different films and reaction conditions is shown in Figure 4. In particular, different deposition orders of the IL and the cobalt precursor were applied at surface temperatures of 110 K and 225 K, respectively. This approach allows studying the influence of the layering in the film on the stability of the precursor against thermal decomposition or oxidation by oxygen or ozone. Our main findings are summarized as follows:

- 1) Preparation of the layered films: Deposition of $\text{Co}_2(\text{CO})_8$ and $[\text{C}_4\text{C}_1\text{Pyr}][\text{NTf}_2]$ at 110 K onto Au(111) leads to layered films consisting of molecular Co carbonyl complexes and IL. We identified several bridged and non-bridged precursor species based on their IR spectra ($\text{Co}_2(\text{CO})_8$ and $\text{Co}_4(\text{CO})_{12}$) and observe dynamic interconversion between these different species. In particular, interaction with Au(111) induces the conversion of CO-bridged complexes to Co carbonyls with exclusively terminal CO ligands.

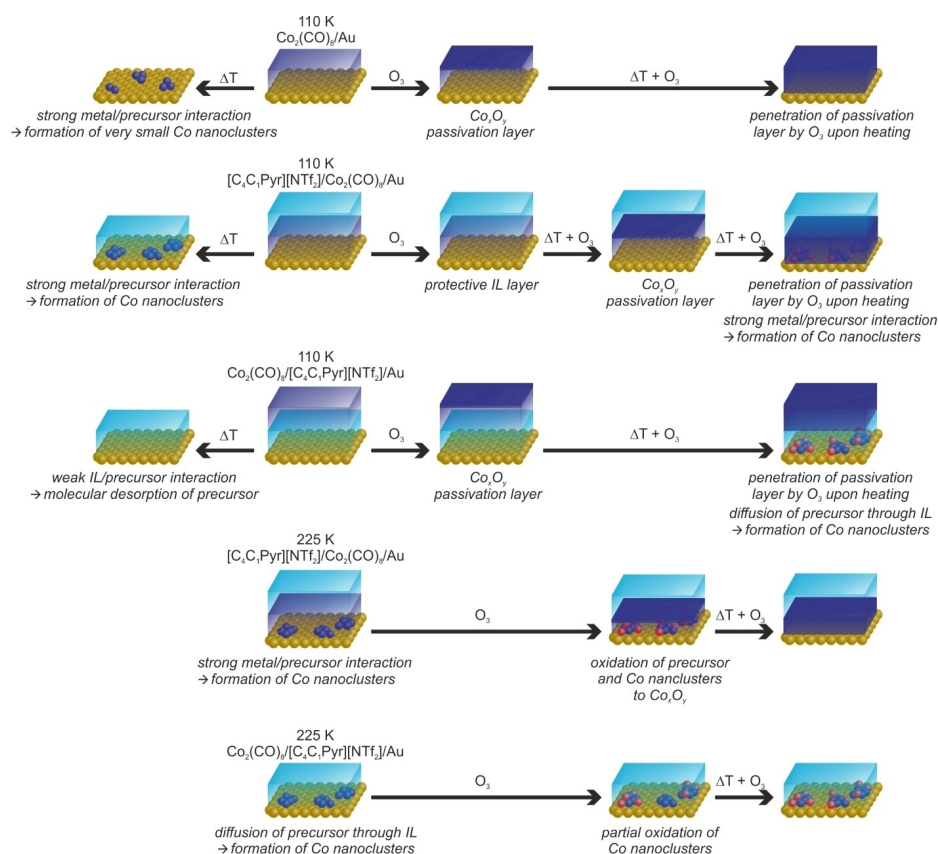


Figure 4. Graphical illustration of the observations for the different films and reaction conditions.

- 2) Thermal stability: The IL/precursor interaction is weak as compared to the interaction of the precursor with Au(111). The comparatively stronger metal/precursor interaction leads to formation of Co nanoclusters on Au(111) upon heating, while the precursor desorbs molecularly from an IL layer. Deposition of $\text{Co}_2(\text{CO})_8$ onto Au(111) or of an IL layer at elevated temperatures (225 K) leads to the formation of Co nanoclusters already during the deposition process.
- 3) Stability against oxidation: Precursor-terminated layers are readily oxidized by ozone at low temperatures. An unordered Co_xO_y layer passivates the films and prevents further oxidation of the precursor molecules. Similarly, also an IL cover layer protects the precursor molecules from oxidation at low temperatures. At elevated temperatures, the oxide passivation layer and the IL get successively permeable for ozone which, in turn, leads to full oxidation of the precursor multilayer. Furthermore, we observe the formation of Co nanoclusters during heating of the systems in ozone.

Acknowledgment

This project was financially supported by the Deutsche Forschungsgemeinschaft (DFG) within the SPP 1708 "Material Synthesis near Room Temperature" (project number 252578361). The authors acknowledge further support by the Excellence Cluster "Engineering of Advanced Materials" in the framework of the

excellence initiative (Bridge Funding). Open access funding enabled and organized by Projekt DEAL.

Conflict of Interest

The authors declare no conflict of interest.

Data availability statement

All experimental data are available from the corresponding author upon request.

Keywords: cobalt oxide · ionic liquids · IR spectroscopy · low temperature synthesis · ozone

- [1] X. Xie, Y. Li, Z.-Q. Liu, M. Haruta, W. Shen, *Nature* **2009**, *458*, 746–749.
- [2] S. Lee, A. Halder, G. A. Ferguson, S. Seifert, R. E. Winans, D. Teschner, R. Schlögl, V. Papaefthimiou, J. Greeley, L. A. Curtiss, S. Vajda, *Nat. Commun.* **2019**, *10*, 954.
- [3] L. F. Liotta, H. Wu, G. Pantaleo, A. M. Venezia, *Catal. Sci. Technol.* **2013**, *3*, 3085.
- [4] Y. Mussa, F. Ahmed, H. Abuhimad, M. Arsalan, E. Alsharaeh, *Sci. Rep.* **2019**, *9*, 44.
- [5] J. Wang, C. Wang, M. Zhen, *Chem. Eng. J.* **2019**, *356*, 1–10.

- [6] C. Schuschke, C. Hohner, M. Jevric, A. Ugleholdt Petersen, Z. Wang, M. Schwarz, M. Kettner, F. Waidhas, L. Fromm, C. J. Sumbly, A. Görling, O. Brummel, K. Moth-Poulsen, J. Libuda, *Nat. Commun.* **2019**, *10*, 2384.
- [7] H. Huang, Y. Xu, Q. Feng, D. Y. C. Leung, *Catal. Sci. Technol.* **2015**, *5*, 2649–2669.
- [8] L. Lukashuk, N. Yigit, R. Rameshan, E. Kolar, D. Teschner, M. Hävecker, A. Knop-Gericke, R. Schlögl, K. Föttinger, G. Rupprechter, *ACS Catal.* **2018**, *8*, 8630–8641.
- [9] Z. Chen, C. X. Kronawitter, B. E. Koel, *Phys. Chem. Chem. Phys.* **2015**, *17*, 29387–29393.
- [10] J. Fester, M. García-Melchor, A. S. Walton, M. Bajdich, Z. Li, L. Lammich, A. Vojvodic, J. V. Lauritsen, *Nat. Commun.* **2017**, *8*, 14169.
- [11] H. Kim, J. Park, I. Park, K. Jin, S. E. Jerng, S. H. Kim, K. T. Nam, K. Kang, *Nat. Commun.* **2015**, *6*, 8253.
- [12] X. Deng, H. Tüysüz, *ACS Catal.* **2014**, *4*, 3701–3714.
- [13] H.-Y. Wang, S.-F. Hung, H.-Y. Chen, T.-S. Chan, H. M. Chen, B. Liu, *J. Am. Chem. Soc.* **2016**, *138*, 36–39.
- [14] F. Faisal, C. Stumm, M. Bertram, F. Waidhas, Y. Lykhach, S. Cherevko, F. Xiang, M. Ammon, M. Vorokhta, B. Šmid, T. Skála, N. Tsud, A. Neitzel, K. Beranová, K. C. Prince, S. Geiger, O. Kasian, T. Wähler, R. Schuster, M. A. Schneider, V. Matolín, K. J. J. Mayrhofer, O. Brummel, J. Libuda, *Nat. Mater.* **2018**, *17*, 592–598.
- [15] C. Xu, Z. Tian, P. Shen, S. P. Jiang, *Electrochim. Acta* **2008**, *53*, 2610–2618.
- [16] T. Bauer, M. Voggenteiter, T. Xu, T. Wähler, F. Agel, K. Pohako-Esko, P. Schulz, T. Döpfer, A. Görling, S. Polarz, P. Wasserscheid, J. Libuda, *Zeitschrift für Anorg. und Allg. Chemie* **2017**, *643*, 31–40.
- [17] B. Uhl, T. Cremer, M. Roos, F. Maier, H.-P. Steinrück, R. J. Behm, *Phys. Chem. Chem. Phys.* **2013**, *15*, 17295.
- [18] C. Schliehe, J. Yuan, S. Glatzel, K. Siemensmeyer, K. Kiefer, C. Giordano, *Chem. Mater.* **2012**, *24*, 2716–2721.
- [19] Y. Jiang, Y.-J. Zhu, *J. Phys. Chem. B* **2005**, *109*, 4361–4364.
- [20] H. Kaper, F. Endres, I. Djerdj, M. Antonietti, B. M. Smarsly, J. Maier, Y.-S. Hu, *Small* **2007**, *3*, 1753–1763.
- [21] J. Dupont, P. A. Z. Suarez, *Phys. Chem. Chem. Phys.* **2006**, *8*, 2441.
- [22] T. Bauer, F. Agel, D. Blaumeiser, S. Maisel, A. Görling, P. Wasserscheid, J. Libuda, *Adv. Mater. Interfaces* **2019**, *6*, 1900890.
- [23] P. Ferstl, S. Mehl, M. A. Arman, M. Schuler, A. Toghan, B. Laszlo, Y. Lykhach, O. Brummel, E. Lundgren, J. Knudsen, L. Hammer, M. A. Schneider, J. Libuda, *J. Phys. Chem. C* **2015**, *119*, 16688–16699.
- [24] T. Xu, M. Schwarz, K. Werner, S. Mohr, M. Amende, J. Libuda, *Phys. Chem. Chem. Phys.* **2016**, *18*, 10419–10427.
- [25] K. Noack, *Spectrochim. Acta* **1963**, *19*, 1925–1931.
- [26] G. Bor, *Spectrochim. Acta* **1963**, *19*, 2065–2073.
- [27] G. Bor, K. Noack, *J. Organomet. Chem.* **1974**, *64*, 367–372.
- [28] R. L. Sweany, T. L. Brown, *Inorg. Chem.* **1977**, *16*, 415–421.
- [29] R. L. Schneider, R. F. Howe, K. L. Watters, *Inorg. Chem.* **1984**, *23*, 4593–4599.
- [30] F. Ungváry, L. Markó, *J. Organomet. Chem.* **1974**, *71*, 283–286.
- [31] G. Bor, U. K. Dietler, *J. Organomet. Chem.* **1980**, *191*, 295–302.
- [32] R. A. Friedel, I. Wender, S. L. Shufler, H. W. Sternberg, *J. Am. Chem. Soc.* **1955**, *77*, 3951–3958.
- [33] Y. Xie, R. B. King, H. F. Schaefer, *Spectrochim. Acta Part A* **2005**, *61*, 1693–1699.
- [34] A. Lagunas, C. Jimeno, D. Font, L. Solà, M. A. Pericàs, *Langmuir* **2006**, *22*, 3823–3829.
- [35] H. Ryeng, O. Gropen, O. Swang, *J. Phys. Chem. A* **1997**, *101*, 8956–8958.
- [36] F. Hoffmann, *Surf. Sci. Rep.* **1983**, *3*, 107.
- [37] R. G. Greenler, D. R. Snider, D. Witt, R. S. Sorbello, *Surf. Sci.* **1982**, *118*, 415–428.
- [38] H. Pearce, N. Sheppard, *Surf. Sci.* **1976**, *59*, 205–217.
- [39] M. Sobota, M. Happel, M. Amende, N. Paape, P. Wasserscheid, M. Laurin, J. Libuda, *Adv. Mater.* **2011**, *23*, 2617–2621.
- [40] M. Sobota, I. Nikiforidis, W. Hieringer, N. Paape, M. Happel, H.-P. Steinrück, A. Görling, P. Wasserscheid, M. Laurin, J. Libuda, *Langmuir* **2010**, *26*, 7199–7207.
- [41] M. Sobota, M. Schmid, M. Happel, M. Amende, F. Maier, H.-P. Steinrück, N. Paape, P. Wasserscheid, M. Laurin, J. M. Gottfried, J. Libuda, *Phys. Chem. Chem. Phys.* **2010**, *12*, 10610.
- [42] C. Schuschke, C. Hohner, C. Stumm, M. Kettner, L. Fromm, A. Görling, J. Libuda, *J. Phys. Chem. C* **2019**, *123*, 31057–31072.
- [43] S. Mehl, P. Ferstl, M. Schuler, A. Toghan, O. Brummel, L. Hammer, M. A. Schneider, J. Libuda, *Phys. Chem. Chem. Phys.* **2015**, *17*, 23538–23546.